A 5-MEV ELECTRON LINAC WITH HIGH ENERGY RESOLUTION

Yu.P. Vakhrushin, V.M. Nikolaev, A.V. Rjactsov,
Yu.A. Svistunov, Yu.P. Severgin, and V.L. Smirnov
D.V.Efremov Scientific Research Institute of
Electrophysical Apparatus, Leningrad, USSR

Summary

The design parameters of a 5-MeV electron linac with low energy spectrum and beam emittance are presented. The accelerator includes the following main components:

(a) an injection system comprising an electron gun, rf chopper, and prebunching cavities,
(b) a traveling-wave accelerating structure operating at room temperature, and
(c) an active monochromatization system with variable longitudinal dispersion.

Three-dimensional numerical studies of beam dynamics were performed taking into account space-charge forces. With the peak current of 3 mA, it is possible to obtain an energy spread less than $\pm 5\times10^{-5}$ and a transverse emittance less than 1 mm-mrad.

Introduction

Electron linear accelerators with high energy resolution are of considerable interest for research in nuclear and high energy physics and for electron microscopy. To date, accelerated beams with the best parameters have been obtained with superconducting linacs;[1] but, the construction of a superconducting linac requires the solution of many technical problems and cannot be considered routine. However, not all the possible ways of improving the beam characteristics in conventional machines have been exhausted. For example; use of an active monochromatization system allowed reduction of the beam energy spread by an order of magnitude for the machines in Mainz[2] and Tokyo.[3]

In this paper, the basic design characteristics are given for a 5-MeV conventional electron linac with a beam energy spread within $\pm 5\times10^{-5}$ and an average accelerated beam current of 15 μA. To meet these specifications, the accelerator has chopper and prebuncher cavities and an active monochromatization system; provision is made for strong stabilization of the basic operating parameters. It is expected that such a machine will be usable in electron microscopy.

Figure 1 shows a schematic layout of the main accelerator components, and a detailed description of the scheme is given below.

Electron Source

A Pierce diode gun with a 2-mm-diameter thermo-emission cathode is chosen as the electron source. The peak current of a continuous beam at the anode plane is 70 mA at the 80-kV cathode-anode voltage. The gun electrode configuration allows the beam diameter to be decreased to 1 and 0.5 mm at the anode and cross-over planes, respectively. In the rest of the accelerator, the beam diameter is maintained at this level by means of the uniform axial magnetic field of ∿ kG produced by the focusing coils.

To reduce the electron transverse momentum gain in the cathode-anode region, it is desirable that the electron trajectories coincide with the magnetic field lines. The required magnetic field distribution is provided by a magnetic shield and bucking coils. The electron flow structure is assumed to be laminar in this region. The coincidence of the magnetic field lines and the electron trajectories is distorted by the electrostatic lens in the anode hole; therefore, the electrons are moving from the anode along spiral trajectories.

The electron dynamics were studied by using a three-dimensional beam model, with the beam represented by a number of small "balls" each of charge q and diameter d. This model was chosen because (1) the rf field in the chopper has no axial symmetry, and (2) the finite beam diameter causes the initial rotational symmetry in charge distribution to be disturbed when electrons cross the slit in the chopper clipping collimator. However; the initial charge distribution at the anode plane is considered to be axially symmetric, both longitudinal $\varepsilon_{\parallel}$ and the transverse $\varepsilon_{\perp}$ emittances being zero (Figs. 2a and 3a).

Chopper and Prebuncher

A well-known system including rf chopper and prebuncher cavities will be used to provide a well-defined electron bunch at the accelerator input. The two-cavity chopper structure suggested by J.P. Mangin[4] was chosen. Its advantages are:

(1) capability of producing short bunches at a relatively low electron energy (up to 100 keV),
(2) restoration of the transverse beam geometry at the chopper output, and
(3) density of heat dissipation in the clipping collimator than with the linear chopping technique.[5]

The 1.5-mm-wide clipping collimator slit transmits an electron bunch with well-defined boundaries and a total phase spread of about 27°. Because the beam diameter is finite, the charge distribution along the bunch is of a trapezium

type with 3-mA peak beam current or 15-μA average at a duty factor of 0.5%.

One of the essential features of the particle dynamics in the chopper is the sharp change in the space-charge forces influencing the particle when it crosses the collimator plane. This change affects mostly the axial motion. In a continuous beam the axial Coulomb field is zero, but in a chopped beam it plays a significant role resulting in essential increase of the longitudinal emittance. Computations show that the limiting value of $\varepsilon_{\parallel}$ is closely approached when the bunch leaves the chopper (Fig. 2b). Additional bunch compression in the prebuncher influences only the shape of the phase-space region occupied by the particles and changes $\varepsilon_{\parallel}$ very little. Thus, the main function of the prebuncher is to transform the longitudinal beam emittance in a manner that allows minimization of high-order aberrations of the accelerator sections. In this case, a prebuncher providing a bunch phase width of 10° and an energy spread of ±2 keV at the accelerator entry (Fig. 2c) was found to be close to optimum. Note that the multi-cavity prebuncher concept shows no essential advantages compared with the single-cavity one.

The transverse (x, x') emittances ε_x at the chopper exit and at the accelerator entry are shown in Figs. 3b and 3c. The ε_x value is changed slightly while the bunch phase width is decreased by a factor of 3.

Accelerating System

The 5-MeV linear accelerator comprises two traveling waveguide sections of identical length (0.9 m). A Klystron providing 5-MW rf peak power and 25-kW average at 2450-MHz frequency is chosen as the rf power source. In waveguide W_1, fed at 3.5 MW, the electrons are accelerated to a nominal energy of 5 MeV. Waveguide W_2, fed at 1 MW maximum, serves to change the energy gain from 3 to 5 MeV. It can also be used to reduce the energy spread if a bunch has any phase-energy correlation, or to provide modulation on particle energies, which is necessary in bunch phase-length measurements.

The rf field in the input coupler cavity and adjacent cells decelerates and defocuses electrons. To reduce this effect, the accelerating field gradient must be comparatively low. Various sets of E(a) and $\beta_w(z)$ curves have been analyzed, where E is accelerating field gradient and β_w is normalized phase velocity. To find the optimum set of these curves, a gradient method[6] was applied which had as a criterion the minimum value of the function

$$F(E,\beta_w) = A\cdot\sum_{i=1}^{N}(\phi_i-\bar{\phi})^2 + \sum_{i=1}^{N}(u_i-\bar{u})^2 \qquad (1)$$

where A is a weight constant; N is the number of particles;

$$\bar{\phi} = \frac{1}{N}\sum_{i=1}^{N}\phi_i;\quad \bar{u} = \frac{1}{N}\sum_{i=1}^{N}u_i;\quad \text{and } \phi_i \text{ and } u_i = \frac{W_i}{m_o c^2}$$

are the phase and the normalized energy of the i^{th} particle at the W_1 exit.

As a result of this analysis, the version was chosen in which the E(z) and $\beta_w(z)$ curves vary smoothly over the ranges 16 to 75 kV/cm and 0.42 to 1, respectively, over the initial part of a W_1 that is 2λ in length (where λ is the rf field wavelength).

The longitudinal and transverse emittances at the accelerator exit are shown in Figs. 2d and 3e. The former remains unchanged during the acceleration time. The latter is reduced, but at a rate slower than the rate predicted by a simple theory, which would be inversely proportional to the longitudinal momentum, because the transverse momentum imparted to the electrons by the rf field in the injection part of W_1, is phase dependent and therefore increases the transverse emittance area.[7] To illustrate this, Fig. 3d shows the transverse emittance at the point $\lambda/2$ downstream from the W_1 waveguide entry, where the average particle energy after deceleration and subsequent acceleration again becomes 80 keV. At this point the ε_x value is nearly twice as large as at the accelerator entrance.

As shown in Fig. 3f, the transverse emittance ε_y in the (y,y') plane at the accelerator exit has a value slightly different from that of ε_x; consequently, the disturbance of the axial symmetry caused by the chopper is of no importance.

Thus, the above analysis confirms that under ideal stability conditions the chosen accelerator scheme allows one to obtain electron bunches with a phase width of 2° and an energy spread of ±0.15%. About 80% of the accelerated particles are within an ellipse of area ε_x = 0.25 mm mrad.

Active Monochromatization System

The energy spread in a bunched beam of charged particles can easily be compensated without intensity losses by using an active monochromatization system. This idea was first proposed by K. W. Robinson[8] and has been tested on the injector for NINA.[9] The bunched beam consisting of relativistic electrons is passed through the achromatic magnet system (debuncher) with high longitudinal dispersion D_{11}. Movement of electrons of different energies along trajectories of different lengths resulted in an elongated bunch, with a linear correlation between particle energy and phase. If such a bunch passes through the rf field at the appropriate phase, the energy spread can be reduced by a large factor.

The active monochromatization system (Fig. 1) consists of a debuncher and two rf compensating cavities C_1 and C_2. The debuncher includes bending

magnets M_1-M_3 and quadrupole lenses Q_3, Q_4. The debuncher magnet system is symmetrical relative to plane AA', and half of it is symmetrical relative to OO'. The optical properties of this system have been studied in a linear approximation by Basargin.[10] The longitudinal dispersion of the debuncher can be regulated by the current variation in lenses Q_3, Q_4, and thus the optimum compensating regime can be chosen for a given energy spread at the accelerator exit. The dispersion D_{11} is determined by

$$D_{11} = R\left[\frac{16.2}{u^2} + 70\left(\frac{\omega_L^2}{\ell} R - 0.795\right)\right], \text{cm} \cdot \left(\frac{\Delta W}{W}\right)^{-1} \quad (2)$$

where R is the trajectory radius in the magnets; u is the normalized particle energy; ℓ is the effective quadrupole lens length; and ω_L is a dimensionless lens parameter.

The magnet field is inhomogeneous in the radial direction with a field index of n = 0.8317 and R = 30 cm. The bending angles are 135° for magnets M_1 and M_3, and 270° for magnet M_2. The quadrupole pair Q_1, Q_2 matches the beam emittance to the debuncher acceptance.

The beam energy spread is eliminated in compensating cavities C_1 and C_2, excited at the frequencies f and 2f respectively, where f is 2450 MHz.

A measure of the system efficiency is the monochromatization factor k_m, defined as

$$k_m = \Delta W_{in}/\Delta W_{out} \quad (3)$$

where ΔW_{in} and ΔW_{out} are the energy spread values at the monochromatization system input and output.

The system can operate in monoharmonic (MHC) as well as biharmonic (BHC) compensation modes. In the MHC mode, only cavity C_1 is energized, and the maximum value k_{m1} is given by

$$k_{m1} = \frac{5}{3}(\Delta\phi_{in})^{-\frac{2}{3}} \quad (4)$$

where $\Delta\phi_{in}$ is the bunch halfwidth at the debuncher input.

In the BHC mode, both the C_1 and C_2 cavities are used, and the maximum value k_{m2} is

$$k_{m2} = 2(\Delta\phi_{in})^{-0.81} . \quad (5)$$

Assuming $\Delta\phi_{in} = 0.02$, in accordance with Fig. 2d, one finds $k_{m1} = 23.0$ and $k_{m2} = 47.7$. The residual energy spread value in the BHC mode is

$$\Delta W_{out} = \pm 7.5/47.7 = \pm 0.16 \text{ keV} .$$

The rf field amplitudes in cavities C_1 and C_2 are 9 kV and 1.5 kV, respectively. The longitudinal emittance of the monochromatic beam is shown in Fig. 2e.

Estimation of the beam properties in the MHC mode shows that elimination of the second-order debuncher aberrations is not required because the emittance values are small; about 80% of the accelerated particles being inside the transverse emittance area of 0.29 mm-mrad. In the BHC mode; however, the chromatic aberrations of the longitudinal motion should be eliminated because of greater bunch elongation. For this purpose, two sextupole lenses should be introduced in the debuncher near lenses Q_3 and Q_4.

Tolerances

To obtain these low values of beam emittances, many of the accelerator parameters should be strictly stabilized. It was determined, in particular, that the tolerable variations of rf power and frequency and of waveguide temperature must be within $\pm 5\times10^{-4}$, $\pm 1\times10^{-6}$, and ± 0.2°C, respectively.

In the monochromatization system, the stability of the bending magnetic field and of the rf field phase in cavity C_1 should be strictly maintained. For example, a change of ±50 eV, in the average electron energy, results from variation either in the magnetic field by 5×10^{-6} or in the rf phase by ±0.3°.

If these tolerances are satisfied, the residual beam energy spread in the BHC mode does not exceed $\pm 5\times10^{-5}$.

Brightness

Brightness B is one of the important parameters of the electron beam used in an electron microscope. Substitution of the average beam current $\bar{i}$ = 12 μA and $\varepsilon_x = \varepsilon_y$ = 0.29 mm-mrad into the brightness equation,

$$B = \bar{i}/\varepsilon_x\varepsilon_y \quad (6)$$

gives B = 14,300 A/cm²-ster. An electron beam with these parameters can be effectively used in an electron microscope of the translucent type.

References

1 J.R. Calarco et al., IEEE Trans. Nucl. Sci. NS-24 (3), 1091 (1977).

2 H. Herminghaus et al., Nucl. Instrum. Methods 113, 189 (1973).

3 M. Sugawara et al., Nucl. Instrum. Methods 153, 343 (1978).

4 G. Azam et al., Onde Electr. 49, 1136 (1969).

5 J. Haimson, IEEE Trans. Nucl. Sci. NS-9 (2), 32 (1962).

6 V.N. Petrov et al., in Proc. 2nd All-Union Conf. on Charged Particle Accelerators, Moscow, Vol. 2, p. 159, 1972.

7 Linear Accelerators, P. 126, P.M. Lapostolle and A.L. Septier, Editors, North-Holland, Amsterdam, 1970.

8 Ibid., p. 512.

9 M.C. Crowley-Milling et al., IEEE Trans. Nucl. Sci. NS-18 (3), 968 (1971).

10 Yu.G. Basargin et al., JETP 42, 1727 (1972).

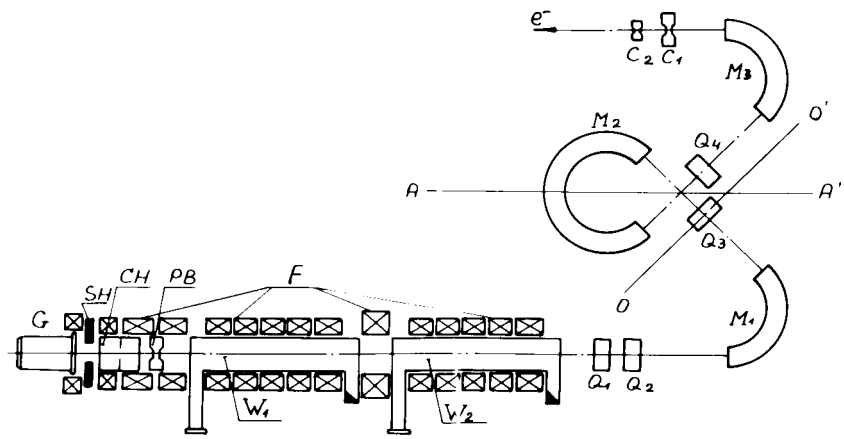

Fig. 1 Schematic layout of the accelerator

G-electron gun; W_1,W_2-accelerating waveguides;
SH-magnetic shield; Q_1,Q_4-quadrupole lenses;
CH-chopper; M_1,M_2-bending magnets;
PB-prebuncher; C_1,C_2-compensating cavities.
F-focusing coils;

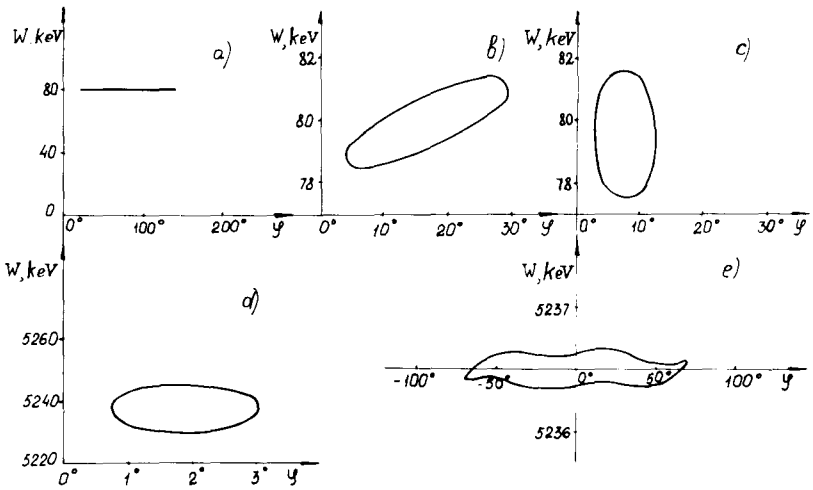

Fig. 2 Longitudinal emittances at different locations along the beam axis

a) in the anode plane;
b) at the chopper exit;
c) at the accelerator entry;
d) at the W_2 waveguide exit;
e) at the monochromatization system exit.

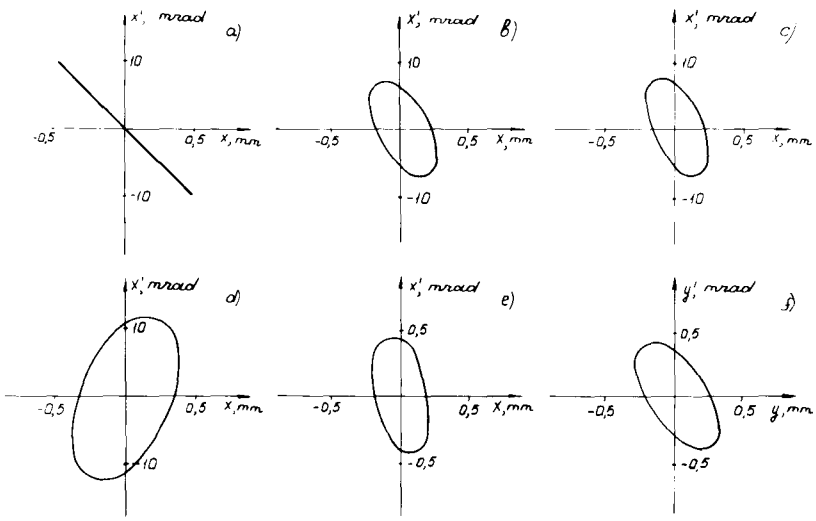

Fig. 3 Transverse emittances at different locations along the beam axis

a) in the anode plane;
b) at the chopper exit;
c) at the accelerator entry;
d) at the point 0.5 downstream of the accelerator entry;
e) at the W_2 waveguide exit, in the (x,x') plane;
f) at the W_2 waveguide exit, in the (y,y') plane.